Development of an Analysis Method for Radial Forging Parameters Based on Hardness Criterion

Saeed Darki[*], *Evgeniy Yurevich Raskatov*
New Material and Technology Institute
Ural Federal University
[*]*saeed.darki@yahoo.com*

ABSTRACT

Considering the complexity of the radial forging process, the study of dynamic and thermodynamic parameters is of great importance. With the severe deformation of a workpiece in a plastic state, the effects of all parameters affecting the final geometry of the forging pipe need to be optimized. Thus, the mathematical model of the process is based on visco-plastic material, taking into account thermomechanical coupling and the surface properties during forging, including the hardness of the workpiece and friction. The results present the effects of a die angle on residual stress, total wear, and contact force, leading to ideal operating conditions and the ideal design of machine parts. In order to ensure the accuracy of the calculations and predictions made through software, a hardness test was performed experimentally, which showed the hardness curve of the microstructure and the strain of the workpiece. This indicates the consistency and accuracy of the results obtained from both methods. In order to improve the process and the tube employed, using an optimized die is recommended.

Keywords: *Finite Element Method; Radial Forging Tube; Residual Stress; Hardness Microstructure; Neutral Plate Coordinate*

Introduction

One tube-forming technique is the Radial Forging Process (RFP), during which the product is surrounded by four dies. This is designed to create round products such as tubes, shafts, stepped shafts, axes, gun bars, and rifle barrels. Reducing the diameter of specimens is the main purpose of radial forging [1]. Accordingly, four dies with special feed rates and rotational angles surround

ISSN 1823-5514, eISSN 2550-164X
Received for review: 2022-06-14
Accepted for publication: 2022-11-16
Published: 2023-01-15

https://doi.org/10.24191/jmeche.v20i1.21084

the specimen. When feeding stops, these dies reduce the diameter and deform the specimen via frequent strokes. Based on these deformations, variations in specimen dimensions in both the radial and axial directions occur. In other words, geometry changes occur in both directions: in the radial direction, which changes the radius, and in the longitudinal direction, which changes the length of the hollow shaft [2].

Farahani et al. [3] found the optimum design profile of the die. Based on this study, they applied two methods of analysis (FEM and the slab method) and compared the results of these two methods for conical and curved specimens. In this comparison between analytical and numerical methods, the results showed only a 6% difference. They also claimed that by increasing the angle and plug angle up to 20°, the normalization of the die presser by plug pressure decreases. In order to estimate the total load except for FEM, the upper bound method can calculate the total force within RFP. Therefore, Groche and Hebdzyński [4]-[5] expressed the relationship between strain and hardening, one of the essential phenomena during cold processes that can directly affect the total load. Studies performed with a sensor element with two separate mandrels have shown that neglecting hardening zone materials with a high hardness coefficient leads to a deviation in the residual stress up to 30%. Designing a radial forging machine and its components, Herrmann et al. [6] and Kocich [7] devised a machine that included four levers and one eccentric sleeve: a ball-and-socket joint supported the levers. Within the new design, they studied the effect of die angle and feed rate, claiming that the forging force decreased. A die surface was designed in order to improve the reduction zone. It was shown that by increasing the amplitude factor, the axial forging force decreases: the designed tools also do not require lubricating material. In addition, Lahoti [8] investigated a multiplier bar within an Al/Cu/Al structure. They analyzed the total force and microstructure behavior through simulation and experiments. According to the results, the total force depends on the length of the multiplier bar, while the maximum force is located at the midpoint in the axial direction. The length of the specimen can affect friction between the various layers. Through an experimental study, Lim et al. [9] presented the microstructure, hardness, and diameters of a bar after the swaging process. Accordingly, they showed that the density of the material increased by decreasing grain size: the hardness and diameter reduction have a direct relationship.

To analyze RS (Residual Stress), strain, and the effect of friction coefficient, Liu et al. [10]-[11] investigated RFP through 2D FEM simulation. Most variations in RS occurred in the axial direction when increasing the feed rate, while the hoop stress criteria are very sensitive to variations in the reduction rate. The final strain is reduced by enhancing the friction value. Due to the nature of RFP, the optimal value of each parameter should be adjusted according to the material and other parameters, but the changing trend is almost constant. Accordingly, the drawing force is decreased by increasing the

die angle; after an increase of almost 6°-8°, the drawing force will increase through the drawing bar [12]. The maximum reduction on the bar and strain hardening are directly proportional. While most scientists have studied this using a 2D mathematical model, this cannot cover all variations during the process.

In this regard, Moumi et al. [13] studied the material flow of the swaging process via FEM. A neutral plate was subjected to a variety of friction and feed velocities. This simulation, based on a 2D cloud, describes various process parameters. By increasing the velocity of feeding, the rate of the neutral plate's location change decreases. One of the essential boundary conditions in order to simulate RFP is the assumed flow material within the process. Therefore, Pantalé and Gueye [14] investigated the Ludwik and Johnson-Cook laws of the behavior of the 2D materials. The elasto-viscoplastic equation is unable to describe the strain rate in cold forging, while the Johnson-Cook law can describe material behavior during cold forging in terms of the strain rate. They show that maximum thickness occurs with a 17% reduction in specimen diameter when operating without a mandrel.

Investigating the microstructure of a forged tube can present the relevant criteria during the process, such as die geometry. The analysis of micro hardness can be used as a validation method. Thus, Sanjari et al. [15]-[17] claimed through a microstructural investigation that by increasing the friction coefficient, the homogeneity of deformation will increase. Moreover, they showed that increasing the friction factor can increase the effective strain: the variations of strain range will increase. The die angle makes the most significant contribution to optimizing the parameters.

Sonmez and Demir [18] measured effective strain values at several points along with a specimen. Therefore, the hardness was calculated via the hardness function and measured values. While FEM produces fewer errors than the upper bound method (based on validation by experimental outcomes), Yang et al. [19] analyzed radial forging with rectangular die and specimens through the upper bound method and FEM. They showed that by increasing the die angle, the axial flow of the material decreases. Due to the wide range of RFP applications, Zhang et al. [20] utilized RFP to join tubular parts. They showed that the length of overlapping could increase the connecting strength; however, if the necking for aluminum increases by more than 45%, the aluminum will fail.

Although FEM and parameter impact have been considered in previous investigations, they have neglected the interaction of parameters with each other or the implementation of the most accurate model and method. Therefore, it is necessary to examine this complex process through variations in the essential parameters that influence the process and to take a comprehensive view of the effects of these changes on the specimen. Therefore, a 3D visco-elastoplastic model was chosen, as it predicts and characterizes this process and all factors affecting it with high accuracy. In

addition, the results were validated through the two parameters of total load and micro hardness. The experimental and simulation results agree, indicating the accuracy of the simulation and prediction process. The equipment for the experiment was located in the metallurgical and rotary machines and organizations of machine-building production in the enterprise Ural NITI (Ekaterinburg).

The parameters and methodology of RFP

RFP is one of the basic tools for metal deformation. This machine includes four dies, which surround the specimen and make consecutive strokes in order to increase material strength. There are many types of radial machines with different functions, such as hot or cold forging, hydraulic or mechanical stroking, and rotary swaging. The radial forging equipment used in the simulation is shown in Figure 1. The mandrel is fixed to the specimens and then four dies deform the product with consecutive strokes.

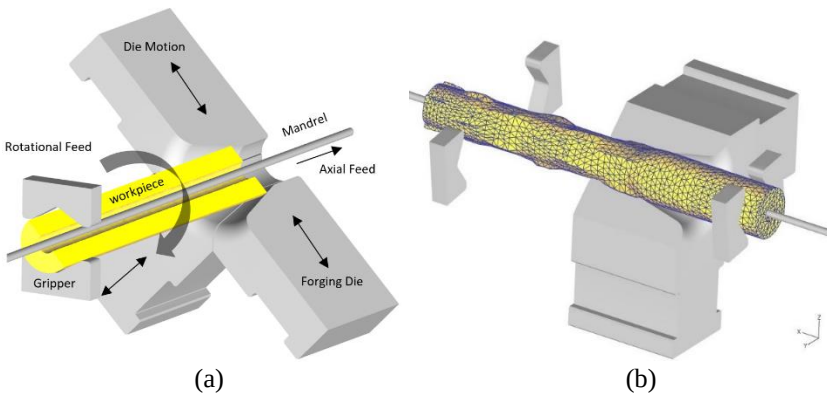

Figure 1: (a) Components and direction of elements in RFP, and (b) the 3D section of simulation with the mesh grid of the workpiece during the simulation process

Quality and dimension precision depend heavily on the process parameters. These parameters directly affect the longevity of the die and forging machine by helping to calculate the residual stress and principal stress on the other components. As such, investigating die geometry through 3D finite element simulation, which can present all interactions between the equipment during operation, is essential. Moreover, regardless of the geometric characteristics of the workpiece, other end-product features, such as residual stress and microstructure, can be affected by the design criteria of the radial forging machine. The geometrical parameters of the die are presented in Figure 2.

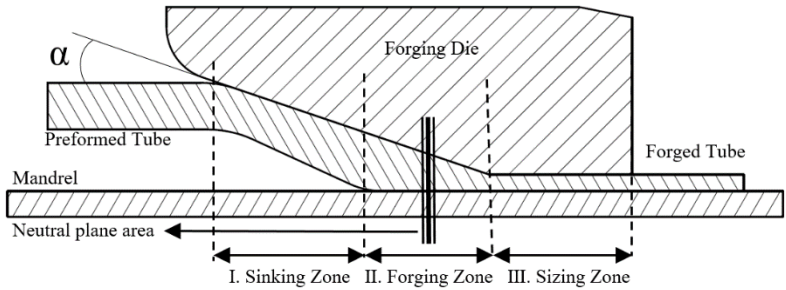

Figure 2. Die angle and three typical zones in the radial forging process

In this figure, the three sections of the die are shown. These have three roles: sinking, forging, and sizing. The die angle has direct effects on sinking and forging. It can also change the coordinates of the neutral plane according to the material flow. The section of the die has a direct relationship with the feed rate and homogeneity deformation of the specimen's surface. The important factors in RFP, such as total force, die angle, type of friction, and value of the coefficient friction, can have a principal role in microstructure hardness, material flow, residual stress, and the amount of increased strength of the specimen. Therefore, these factors are discussed below via a comparison between different types of friction and the value of parameters.

Two types of friction are considered: Coulomb (sliding) and constant shear (sticking). The coulomb law describes the contact forces between two objects under elastic deformation. However, these objects can be elastic-plastic: one is elastic and the other is rigid during elastic deformation. Moreover, the simulation of sheet forming is recommended. Frictional stress is calculated to describe the contact of two plastic or porous objects by the flow stress of the object. The frictional force in the Coulomb's law model is defined via:

$$f_s = \mu P \tag{1}$$

where f_s is frictional stress, P is the interface pressure between two bodies, and μ is the friction factor. Constant shear friction includes highly precise measurement and modeling of bulk-forming simulations. The frictional force in the constant shear law is defined as follows:

$$\tau = m\sigma_y/\sqrt{3} \tag{2}$$

where m is the frictional coefficient and σ_y is the normal yield stress of the material. This states that friction is a function of the yield stress of the deforming body.

The steel DIN-16CrMo4 is considered to create mathematical modeling and simulation. The material parameters are as follows (Table 1).

Table 1: Mechanical properties of the used material

Density (kg/m3)	7870
Young's modulus (GPa)	212
Poisson's ratio	0.3
Specific heat (J/kg/· C)	750
Conductivity (W/m/· C)	15
Melting temperature (C)	1450-1510
Inelastic heat fraction	0.9
Thermal expansion coefficient (1/· C)	11×10^{-5}
Yield Strength (Mpa)	275

Regarding the primary boundary condition for the workpiece, a temperature of 900 °C was used to begin the forging process. This is the primary temperature recommended by previous studies, a necessary experimental condition in order to keep the mechanical properties of the material, and the best temperature for the forging process. In addition, the mathematical model of flow stress is driven by the Johnson-Cook equation:

$$\bar{\sigma} = (A + B\bar{\varepsilon}^{n})\left(1 + C\ln(\frac{\dot{\bar{\varepsilon}}}{\dot{\bar{\varepsilon}}_0})\right)\left(\frac{\dot{\bar{\varepsilon}}}{\dot{\bar{\varepsilon}}_0}\right)^{\alpha}(D - ET^{*m}) \quad (3)$$

where $T^{*} = \left(\frac{T - T_{room}}{T_{melt} - T_{room}}\right)$ and $(\bar{\sigma})$ is the material flow stress. Effective plastic strain rate $(\dot{\bar{\varepsilon}})$ and (T_{melt}) are at melting temperature. $A, B, C, D, E, n, \alpha, \dot{\bar{\varepsilon}}_0$ are model coefficients of the material, and T , m are the thermal softening of the material. A flow stress chart is presented in Figure 3.

As mentioned, parameters such as residual stress can have a direct impact on the strength of the specimen and its longevity. Residual stress is a function of multiple factors such as temperature, die angle, total force, and friction: thus, the effect of these factors is presented and analyzed separately. Thus, material flow velocity, one of the factors used for calculating the microstructure of the material and the amount of hardness, is examined in the following sections. Moreover, the effect of die angle on the neutral plane coordinates via material velocity and the location of the neutral plane relative to the die zone are presented. In terms of friction, the effects of different values of coefficient friction on temperature, residual stress, and specimen quality are shown. The most accurate and most suitable types of friction have been determined by comparing the simulation results for two types of friction and their effect on forging force. It is worth mentioning that the type of friction has been determined using the simulation results closest to the actual results. In

this investigation, the simulation has been validated by comparing experimental hardness values and simulated hardness values. Specimen hardness itself is a function of different parameters, however; it is expressed here using temperature and effective strain. For this purpose, a hardness test was designed to measure hardness at several points along the specimen. Finally, as simulation verification, the experimental and measured graphs were compared. Other outcomes of the simulation could be cited, such as residual stress and the analysis of other influences on specimen quality.

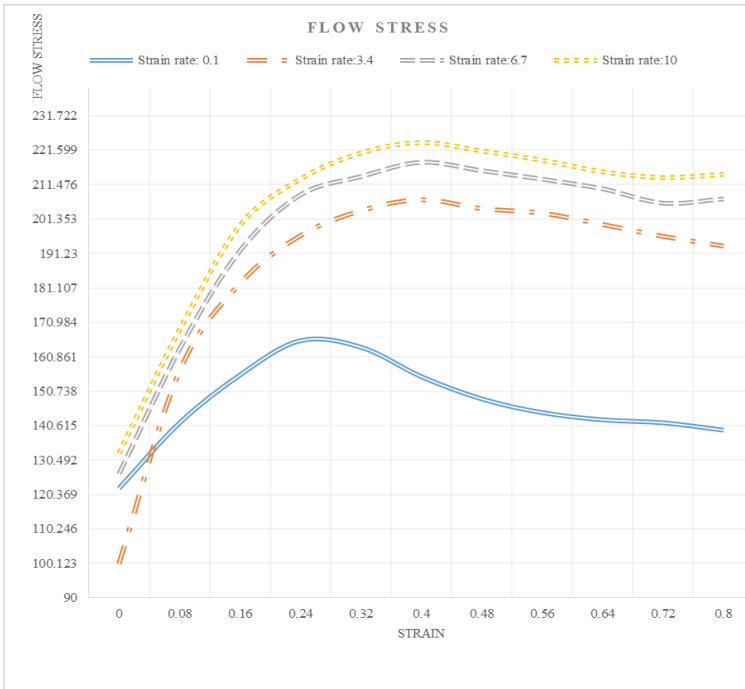

Figure 3. Flow stress-strain curve of the DIN-16CrMo4 steel at 900 ˚C

In general, due to the complex nature of the process, which is a function of overlapping multiple factors, there is no explicit concept of optimization for the whole process. When expressing an optimal value for die angle, total force, or feed rate, other parameters may be neglected. Thus, it seems that the best way to study this process is a comprehensive analysis of the effects of the parameters on each other. Due to the wide potential application of this process, it is worthwhile attempting to increase the quality of the specimen and meet working conditions.

Numerical analysis and experimental method

There are several methods for analyzing the forging process, such as the upper bounds methods, the slab method, and others investigated and implemented by previous authors: however, the most accurate results were obtained by FEM using 3D Deform software. This method provides a comprehensive view of all the phenomena and conditions during forging.

By applying appropriate boundary conditions and simulation parameters, simulation accuracy can be significantly increased. Therefore, conditions such as friction in all process components (the back spring pressure of manipulators and the mandrel and their impacts on material flow) are considered. Using specimen temperature, the heat transfers of the mandrel and the specimen have been calculated: this can have a direct effect on specimen hardness. Therefore, the visco-plastic model has been used for a more accurate examination of the material flow rate. The Von Mises yield criterion has been implemented in order to determine the flow rules. Darki et al. [1] have presented the relation between the essential matrices of FEM.

Although other models such as the rigid plastic or elastoplastic ones have been used in most previous studies, these do not have the necessary precision to determine neutral plate coordinates. In other words, it can be stated: (i) the viscoelastic properties have been considered for workpieces; (ii) there is heat transfer during the forging process; and (iii) the other components of the forging machine have been assumed to be rigid materials, including the dies and mandrel. The final stress after each stroke on the product is defined as residual stress within the final product.

In order to investigate the effects of the die angle, six different specimens are considered: these are described in the following Table 2. Other geometrical dimensions of the components are listed in Table 2. It should be noted that all measurements in the simulation after each stroke have been taken into account to show that stroke effect remains the same over the length of the tube. The length of the specimen is 200 mm. The simulation dynamic parameters, such as rate of stroking (stroke per min), rotating feeds, axial feed (mm), number of strokes, number of passes, and rotations per pass, are respectively; 400, 36°, 20, 12, 2, and 10°.

Table 2: Dimensions of the components of radial forging machine

Outer diameter – Reduction rate	30mm – 20%
Inner diameter – Reduction rate	10mm – 60 %
Outer diameter for mandrel	4mm
Length of die	70mm
Length of die land	25mm
Die angle	5°, 10°, 12.5°, 15°, 20°, 90°

To validate the simulation, the hardness criterion is measurable. For this purpose, two auxiliary criteria, effective strain and temperature, have been used. These two criteria have an impact on the hardness of the specimen as illustrated in Figure 4. For this reason, a tube with the geometry of the simulated specimen is used. A hardness tester measured the length, radius, and thickness of the sample. The following is a view of the measured sample.

Figure 4: The specimen of the tube for the hardness test

The experiment used standard temperature conditions and a portable hardness tester to measure the hardness in different sections at random points. According to the dimensions of the tube, the impact device type D was considered for measuring the hardness of the tube in different sections through the variations of effective strain. For this purpose, about 50 points were marked and measured. It should be noted that the die angle for this test was 5°. After measuring the radius variations and calculating the effective strain on the sample, the hardness-strain curve was obtained. The effective strain equation is given below [2].

$$\overline{\varepsilon} = \frac{\sqrt{2}}{3}\sqrt{(\varepsilon_1 - \varepsilon_2)^2 + (\varepsilon_2 - \varepsilon_3)^2 + (\varepsilon_3 - \varepsilon_1)^2} \tag{4}$$

where $\varepsilon_{1,2,3}$ are the principal strains and $\overline{\varepsilon}$ is the effective strain. By measuring the different strains on the specimen through simulation and placing them into the hardness function, the hardness value of the specimen is shown. To apply the temperature effects to other types of die and to show the distribution of hardness in all sections of the specimen, the hardness-temperature curve was defined by the hardness values obtained for different strains and temperature values. The hardness distribution is thus rendered visible by the temperature and strain effects. After comparing the experimental and simulation results and verifying the accuracy of the simulation, the same method of simulation was used to analyze the other parameters. The following equation expresses the hardness function, where (Hv) is hardness and ($\bar{\varepsilon}$) is effective strain.

$$Hv = -60.7\bar{\varepsilon}^2 + 119.1\bar{\varepsilon} + 115.1 \quad (5)$$

In terms of the comparison between the error percentage of the simulation and experimental results, the current simulation procedure can be used for developing and expanding the investigation of parameters such as coefficient friction and die geometry. This simulation has been verified by comparing it with experimental results for cold RFP, which is presented in Table 3 [1].

Table 3: Specimen geometry and contact force via the experimental and simulation results of process [1]

Sample type	Outer radius of perform (mm)	Inner radius of preform (mm)	Out radius of product (mm)	Inner radius of product (mm)	Die force (KN)
Experiment	18	14.6	13.70	9.30	385.00
FEM	18	14.5	13.66	9.45	366.480

Based on the methodology section and Table 3, the dimensions of the experimental and mathematical models for a cold forging sample are illustrated. According to the obtained results, a good correspondence is established between the practical and FE model results in terms of contact force. In Figure 5, it is shown that a radial forging machine can produce experimental contact force. The difference in the obtained results is less than 5%, which might be due to a thermal effect. In this figure, two different parts of the radial forging machine are shown. Figure 5a shows the position of the workpiece relative to the die and hammer and the location of the workpiece and the feeding device. Figure 5b shows a side view of the machine to present the shape of the die, die angle, and zones of the die.

In order to measure the contact force between the die and the workpiece, two different methods have been considered based on experimental testing and FEM. During the experimental testing, in the case of contact force, the radial forging machine has the ability to calculate the contact force: the diameter is measured by the operator manually. Likewise, for FEM, commercial software can calculate the contact force at each step: the deformation and reduction of the diameter can be measured by the simulation. The stress and wear distribution on the die and workpiece can be calculated.

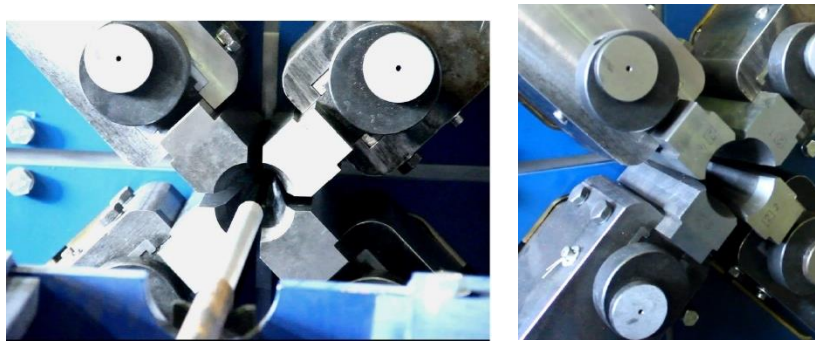

(a) (b)

Figure 5: Radial forging machine with a feeding system during the practical test

Results and Discussion

Since the contact force is one of the principal criteria of RFP in order to analyze the process, the examination of contact force vs radius reduction leads to an estimate of the quality of the created tube and the dimensions of the radial machine. Therefore, Figure 6 displays the contact force in the experimental results [9] and the FEM results vs the reduction to the outer radius of tube. This has been obtained to estimate applied force vs reduction radius for the used material. According to this comparison, the current simulation results have less error than other methods and previous investigations [16].

The importance of force calculation is twofold. First, force is the most fundamental parameter in the forging process: on its basis, the validation of the simulation and calculations can be confirmed. Second, the changes in the force parameter in relation to the reduction of the workpiece's diameter and the prediction of the required force for the design of the forging process can be shown. Therefore, the die contact force is shown based on the changes to the diameter of the workpiece: this can be used to verify the simulation. The force change function, based on the reduction of the tube diameter, needs to be obtained for other designs in order to give a criterion for predicting the total force of the process.

Die angle impacts

In Figure 7, the effective strain distribution along the specimen at different angles is displayed. The most uniform deformation belongs to the 15° angle. The 5° and 90° angles have the highest strain oscillations, indicating surface non-uniformity.

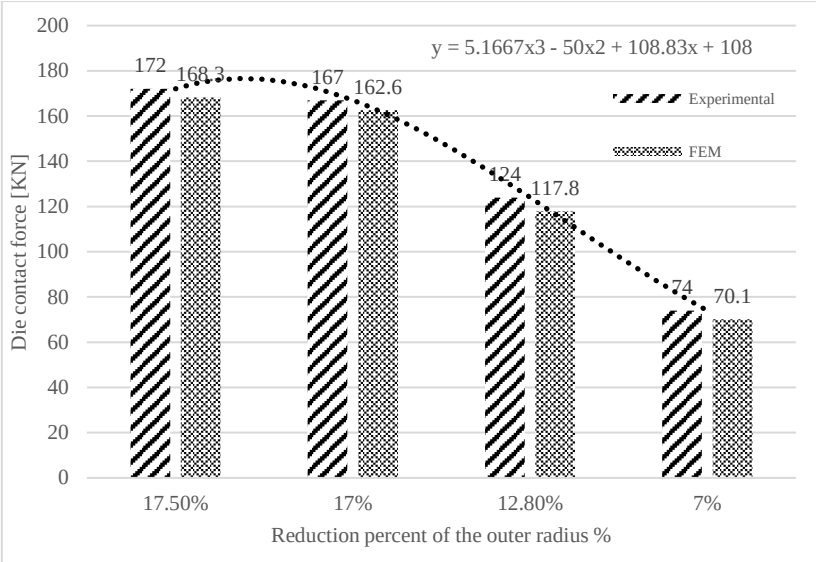

Figure 6: The reduction radius rate vs applied force with an estimate by a 3-degree polynomial function

Sanjari et al. [16] claimed that at an angle of 5°, the neutral plate is in the forging section. According to the obtained results, as the angle increases, the position of the neutral plate moves from the size section to the forging section. Similarly, as the angle decreases, the distance of the neutral plate from the edge of the pipe increases. On the other hand, as the die angle increases, the angle of the distribution of velocity zones in the material increases (β), which in turn can affect the shape of the granular material, thereby establishing a criterion for describing the microstructure. Figure 8 illustrates this phenomenon, the variation of the angles of the material flow layers, and the position of the neutral plate.

Just as angle changes have different effects on the specimen, these changes can also occur in the forging machine. Residual stress is an important parameter in die analysis. For this purpose, the maximum stroke amplitude for different angles in the first pass was considered and the residual stress in the same motion range calculated.

These variations are displayed in Figure 9. According to the results, the lowest value is produced by an angle of 12.5°. After this angle, the residual stress on the die increases significantly. There are no drastic changes for angles lower than 12.5°.

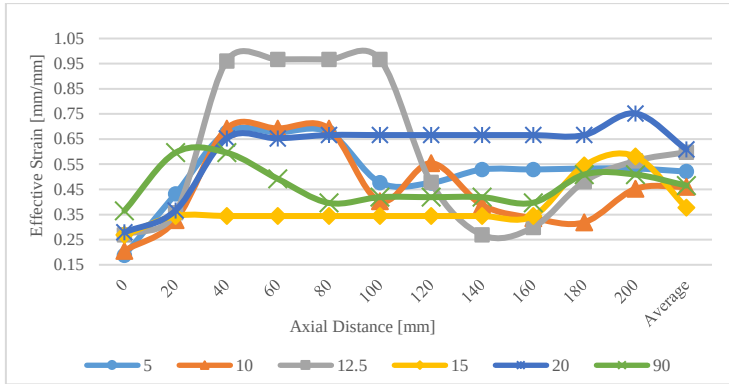

Figure 7: Distribution of effective strain along the specimen at different die angles

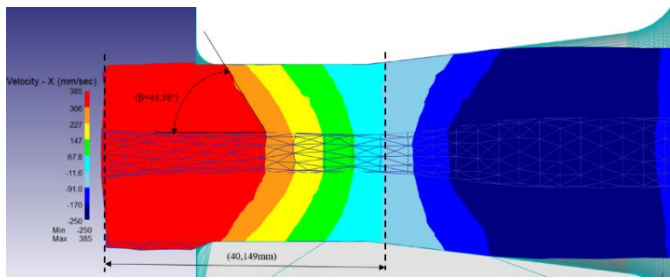

(a)

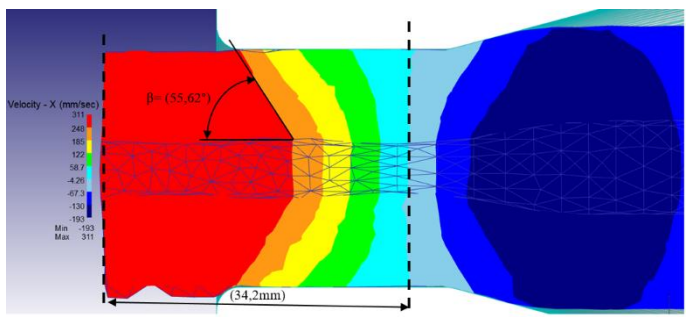

(b)

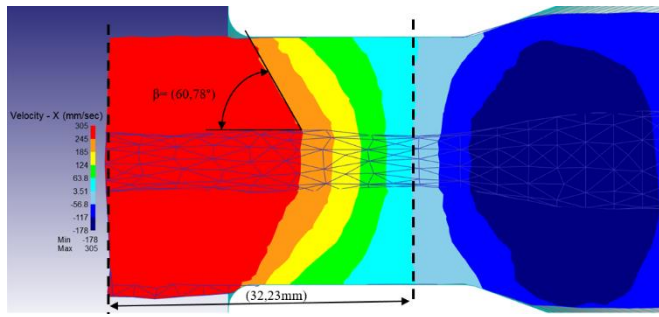

(c)

Figure 8: (a) 5 die angles, (b) 15 die angles, and (c) 20 die angles vs the distribution of velocity and the distance between the end of the specimen, the neutral plane, and the angle of velocity

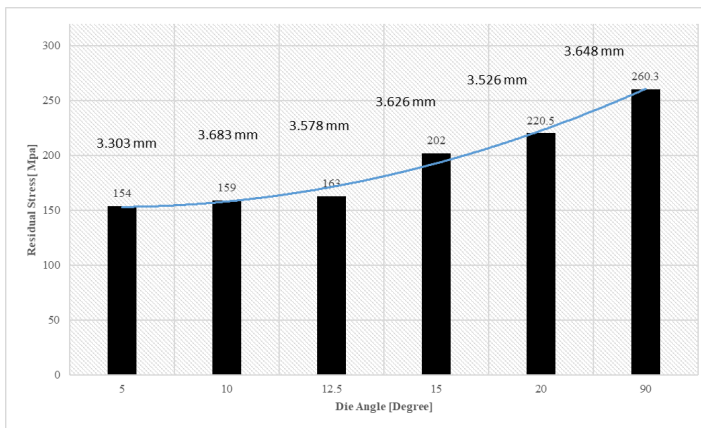

Figure 9: Die distribution of residual stress at maximum strokes at different die angles

Hardness

Tube hardness analysis here consists of two parts: analysis of the experimental results and analysis of the simulation results. In the experimental section, after calculating the effective strain value and measuring the hardness of the specimen with a hardness tester, the curves of the effective strain and hardness were obtained. Figure 10 expresses the strain-hardness curve obtained via 4 approximated polynomials. Similarly, Figure 11 shows that the measured values by a hardness tester were between 0.2-0.3 mm/mm effective strain. Finally, the investigation and analyses have been validated by comparing the hardness-strain curve obtained through the simulation and the experiment.

Given the strong agreement between the simulation and experimental results, it can be claimed that other simulation results are reliable for analyzing radial forging in industrial conditions.

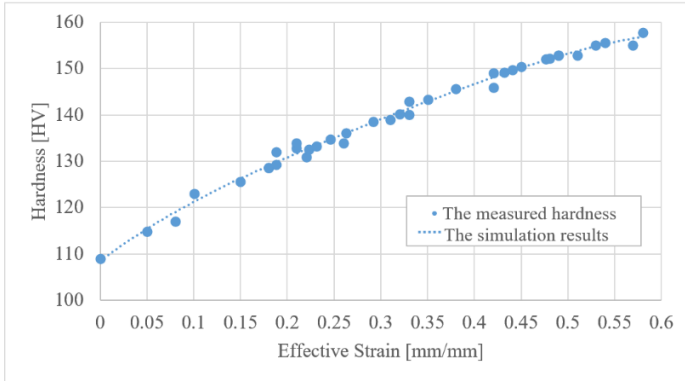

Figure 10: Comparison of the hardness-strain experimental curve (measurement) and simulation values by an approximate fourth-order polynomial

Figure 12 shows the hardness distribution on the specimen's surface along the longitudinal line. According to the results, the lowest value for hardness distribution on the surface is produced by an angle of 15°. On the other hand, this angle leads to the highest hardness uniformity. The uniformity of the hardness distribution can be a criterion of microstructure quality and the uniformity of granularity in the surface layers.

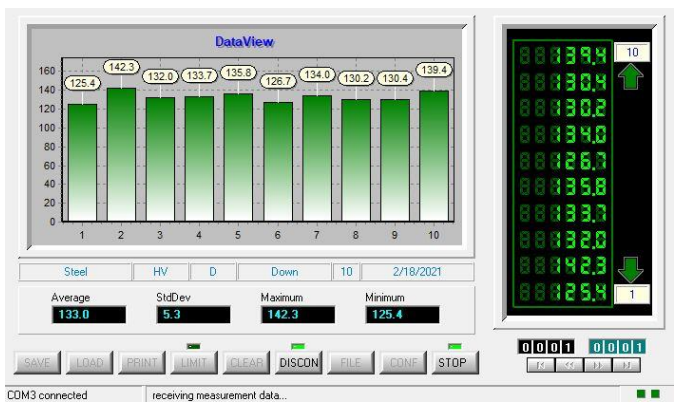

Figure 11: The display of measured values by a tester on a computer

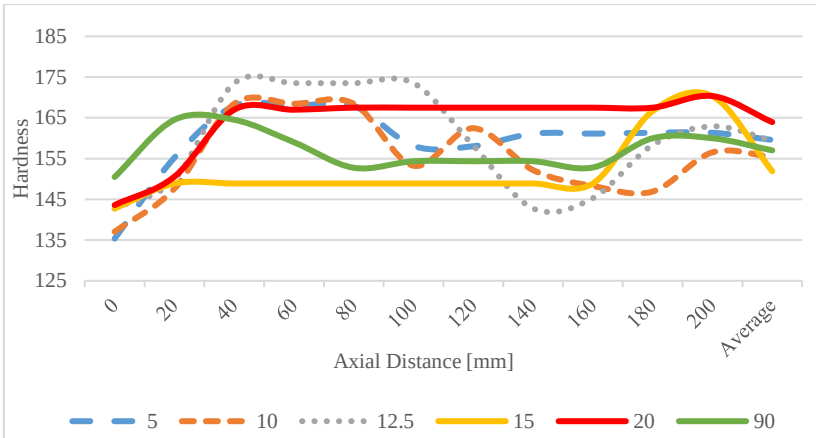

Figure 12: Distribution of hardness along the specimen at different die angles

According to the calculations and simulation, the relationship between the die angle and the effective strain is shown along the length of the tube. Moreover, the lowest effective strain rate is produced by an angle of 15 degrees, which is shown in Figure 7. The relationship between the effective strain and the hardness of the tube is illustrated in Figure 10. The hardness of the workpiece increases as the effective strain increases by an approximate fourth-order polynomial. For this reason, it can be concluded that an angle of 15 degrees produces the lowest strain rate and thus has the lowest level of hardness.

Conclusion

In this research, a three-dimensional model of a radial forge was simulated and subjected to numerical analysis based on FEM. The simulation and experimental results were compared to each other. The strong agreement of the obtained results indicates the accuracy of the simulation for analysing and predicting the characteristics of specimens based on the required conditions. In this research, an attempt has been made to analyse all the parameters affecting this process in order to provide the specimen with the required characteristics.

To investigate the current forging process further, other parameters can be analysed after improving the quality of the workpiece, such as the die stress and the wearing of the die. In addition, the improvement of different shapes of die by taking into account the wear rate and stress of the die can be recommended. Therefore, the results can be summarized as follows:

i. As the die angle increases, the angle of the velocity layers (β) in the material increases. This can reduce the distance between the neutral plate and the end of the specimen, transferring it to the sizing area. As a result, the radial force increases.
ii. Increasing the die angle increases residual stress in the die. Thus, for angles above 12.5°, residual stress in the die increases considerably, which indicates a decrease in the longevity of the die and an increase in die fatigue.
iii. The highest hardness is obtained at an angle of 20°, which creates uniform hardness along the entire length of the specimen. The amount of hardness changes greatly at other angles.

Contributions of Authors

The authors confirm the equal contribution in each part of this work. All authors reviewed and approved the final version of this work.

Funding

This work received no specific grant from any funding agency.

Conflict of Interests

All authors declare that they have no conflicts of interest.

References

[1] S. Darki and E. Y. Raskatov, "Analysis of the hot radial forging process according to the finite element method," *The International Journal of Advanced Manufacturing Technology*, vol. 110, no. 3–4, pp. 1061–1070, 2020.
[2] V. Deform and P. C. Documentation, "DEFORM V11.0 (PC) Documentation," vol. 1. Instruction and tutorial of 3D Deform software.
[3] N. D. Farahani, A. Parvizi, A. Barooni, and S. A. Naeini, "Optimum curved die profile for tube drawing process with fixed conical plug," *The International Journal of Advanced Manufacturing Technology*, vol. 97, no. 1–4, pp. 1–11, 2018.
[4] P. Groche and M. Krech, "Efficient production of sensory machine elements by a two-stage rotary swaging process—Relevant phenomena

and numerical modelling," *Journal of Materials Processing Technology*, vol. 242, pp. 205–217, 2017.
[5] R. Hebdzyński, S. Kajzer, and R. Kozik, "Forging on the four-lever arms swaging machines," *Journal of Materials Processing Technology*, vol. 64, no. 1–3, pp. 199–206, 1997.
[6] M. Herrmann, C. Schenck, and B. Kuhfuss, "Dry Rotary Swaging with Structured Tools," *Procedia CIRP*, vol. 40, pp. 653–658, 2016.
[7] R. Kocich, L. Kunčická, C. F. Davis, T. C. Lowe, I. Szurman, and A. Macháčková, "Deformation behavior of multilayered Al-Cu clad composite during cold-swaging," *Materials and Design*, vol. 90, pp. 379–388, 2016.
[8] G. D. Lahoti and T. Altan, "Analysis of the radial forging process for manufacturing rods and tubes," *American Social Mechanical Engineers*, vol. 98, no. 1, pp. 265–271, 1975.
[9] S. J. Lim, H. J. Choi, and C. H. Lee, "Forming characteristics of tubular product through the rotary swaging process," *Journal of Materials Processing Technology*, vol. 209, no. 1, pp. 283–288, 2009.
[10] L. Liu and L. Fan, "Study of residual stresses in the barrel processed by the radial forging," *2009 2nd International Conference on Information Computing Science ICIC 2009*, vol. 4, pp. 131–134, 2009.
[11] Y. Liu, M. Herrmann, C. Schenck, and B. Kuhfuss, "Plastic Deformation Components in Mandrel Free Infeed Rotary Swaging of Tubes," *Procedia Manufacturing*, vol. 27, pp. 33–38, 2019.
[12] M. M. Mahdavi and H. Haghighat, "On the Optimum Die Angle in Rod Drawing Process Considering Strain- hardening Effect of Material," *Iranian Journal of Mechanical Engineering*, vol. 20, no. 1, pp. 113-128, 2019.
[13] E. Moumi, S. Ishkina, B. Kuhfuss, T. Hochrainer, A. Struss, and M. Hunkel, "2D-simulation of material flow during infeed rotary swaging using finite element method," *Procedia Engineering*, vol. 81, pp. 2342–2347, 2014.
[14] O. Pantalé and B. Gueye, "Influence of the constitutive flow law in FEM simulation of the radial forging process," *Journal of Engineering*, vol. 2013, pp. 1-8, 2013.
[15] M. Sanjari, A. Karimi Taheri, and A. Ghaei, "Prediction of neutral plane and effects of the process parameters in radial forging using an upper bound solution," *Journal of Materials Processing Technology*, vol. 186, no. 1–3, pp. 147–153, 2007.
[16] M. Sanjari, P. Saidi, A. Karimi Taheri, and M. Hossein-Zadeh, "Determination of strain field and heterogeneity in radial forging of tube using finite element method and microhardness test," *Materials and Design*, vol. 38, pp. 147–153, 2012.
[17] M. Sanjari, A. K. Taheri, and M. R. Movahedi, "An optimization method for radial forging process using ANN and Taguchi method," *The*

International Journal of Advanced Manufacturing Technology, vol. 40, no. 7–8, pp. 776–784, 2009.

[18] F. O. Sonmez and A. Demir, "Analytical relations between hardness and strain for cold formed parts," *Journal of Materials Processing Technology*, vol. 186, no. 1–3, pp. 163–173, 2007.

[19] X. Yang, X. Dong, and Y. Wu, "An upper bound solution of forging load in cold radial forging process of rectangular cross-section billet," *The International Journal Advanced Manufacturing Technology*, vol. 92, no. 5–8, pp. 2765–2776, 2017.

[20] Q. Zhang, Y. Zhang, M. Cao, N. Ben, X. Ma, and H. Ma, "Joining process for copper and aluminum tubes by rotary swaging method," *The International Journal of Advanced Manufacturing Technology*, vol. 89, no. 1–4, pp. 163–173, 2017.